Local magnetic behavior of Rh in Ni-Rh alloys: An experimental and theoretical study

V. V. Krishnamurthy, S. N. Mishra, M. R. Press, P. L. Paulose, S. H. Devare, and H. G. Devare
Tata Institute of Fundamental Research, Homi Bhabha Road, Bombay 400 005, India
(Received 1 June 1993; revised manuscript received 4 October 1993)

Magnetic behavior of Rh in paramagnetic Ni_xRh_{1-x} for $x \leq 0.63$ is studied by measuring the ^{100}Rh local susceptibility using the time-differential perturbed-angular-correlations method, the bulk magnetization, and through local-spin-density calculations. For $x \sim 0.6$ the measured Curie-Weiss local susceptibility yields a high Rh magnetic moment with a small spin-fluctuation temperature ≤ 100 K, while for $x \lesssim 0.40$ the observed results are consistent with an unstable moment on Rh characterized by large spin-fluctuation temperatures $\sim 10^3$ K. The magnetism of Rh in the Ni-Rh system is found to depend on the number of Ni atoms in its immediate surrounding. The calculations show that both Ni and Rh atoms acquire moments in the presence of at least two Ni atoms in the nearest-neighbor (NN) coordination shell. Further, Ni and Rh moments are found to depend on the geometrical arrangement of the NN Ni atoms. The increase in the moment value on individual atoms and the enhanced susceptibility comes from the growing proportion of three-dimensional or isotropic NN Ni configurations over the linear or planar configurations, which occur for 5–6 or more Ni atoms. Our experimental results, as well as theoretical calculations, show that Rh magnetic behavior is strongly influenced by the sign of the interatomic exchange interaction. In particular, the observed enhanced Rh magnetic response near $x \sim 0.6$ is attributed to the ferromagnetic d-d interaction between Rh and Ni atoms.

I. INTRODUCTION

Magnetic behavior of 4*d* ions in transition metals, alloys, and in metal overlayers continues to generate a great deal of interest leading to an increasing number of experimental and theoretical studies over the last few years. Recently, with the help of time-differential perturbed-angular-correlation and perturbed-angular-distribution (TDPAC and TDPAD) techniques, in combination with the recoil-implantation method, it has been possible to study the occurrence of 4*d* magnetic moments and to measure their spin-fluctuation rates in many different hosts. Measurements in host containing *d*-band electrons and exhibiting exchange-enhanced susceptibility, e.g., Pd and Pt, have revealed the existence of a large quasistable magnetic moment on Ru and Rh impurities.[1–3] Further, it has been observed that the 4*d* spin-fluctuation rates and hence the magnetic-moment stability strongly depends on the sign and strength of the impurity *d*-host *d* interaction.[3,4] As far as the magnetism of 4*d* ions in transition-metal hosts is concerned, most of the experimental work is limited to Pd and Pt and their dilute alloys. It is therefore of interest to study the magnetism of 4*d* ions in other transition-metal hosts with large exchange enhanced *d*-band susceptibilities to explore the possibility of the occurrence of 4*d* magnetic moments in such systems.

The magnetic system Ni_xRh_{1-x} is known to be paramagnetic below a critical composition $x_{crit}=0.63$; close to this composition it exhibits high exchange-enhanced bulk susceptibility with large Stoner factors[5] estimated to reach ~ 70. The enhanced *d*-band susceptibility in this system has been studied by measuring the magnetic behavior of dilute Fe in $Ni_{0.63}Rh_{0.37}$, which shows the occurrence of giant magnetic moment of $\sim 12\mu_B$ per Fe atom, similar to the behavior of Fe in Pd, thus making the system an ideal choice for the study of magnetism on the 4*d* Rh atom. Using ^{103}Rh Knight-shift and spin-lattice relaxation rate data obtained from NMR measurements, Narath and Weaver[6] demonstrated that addition of Ni to Rh causes a large increase in the Rh *d*-spin polarization and argued that the enhancement in local susceptibility is caused due to the changes in the local density of states near the Fermi energy. From the temperature and field dependence of the magnetization of Ni-Rh alloys near the critical composition $x=0.63$, Muellner and Kouvel[7] attributed the onset of ferromagnetism to the divergence of the Curie-Weiss susceptibility component due to ordering interactions between super paramagnetic clusters. These clusters, carrying an average moment $\gtrsim 20\mu_B$, increase rapidly in concentration as $x_{crit}=0.63$ is approached. In view of these results and the different interpretations, more detailed microscopic investigations to study the magnetic behavior of Rh in this system are desirable.

The time differential perturbed angular correlation (TDPAC) method[8] is one of the most suitable techniques for such magnetic studies. Apart from the measurement of local susceptibility, this method allows, in suitable cases, measurement of nuclear spin relaxation rates at any temperature which can be related to the spin fluctuation properties of the probe atom. Further, the technique is quite sensitive to small changes in the immediate surrounding of the probe atom so that the measured local susceptibility data can be correlated to the near neighbor effects.[3,4] Hitherto, such studies using TDPAC technique have not been made for the Ni-Rh system.

In this paper we present our results on the magnetism of Rh in the alloy system Ni_xRh_{1-x} obtained from bulk magnetization studies and ^{100}Rh local susceptibility mea-

surements using the TDPAC method. Complementing the experimental studies, we have also performed local spin density calculations using the linear combination of atomic orbitals forming molecular orbitals (LCAO-MO) method to estimate the spin magnetic moments on Ni and Rh atoms in Ni-Rh alloys as a function of nearest-neighbor Ni and Rh atom coordination. Our results show large spin magnetic moment for Rh- in the Ni-rich alloys with $x \sim x_{crit}$, while in the Rh rich alloys the results are consistent with the existence of an unstable magnetic moment on Rh characterized by a high-spin fluctuation temperature. They also indicate that the Rh magnetic moment and its stability varies strongly with the number of Ni atoms in the near-neighbor shell. Preliminary experimental results of ^{100}Rh local susceptibility and bulk magnetic susceptibility for $Ni_{0.6}Rh_{0.4}$ have been presented elsewhere.[9]

In Sec. II we briefly discuss the experimental techniques and the results are presented in Sec. III. Theoretical calculations using the LCAO-MO method are presented in Sec. IV, followed by a discussion of our results and conclusions in Sec. V.

II. EXPERIMENTAL APPROACH

Polycrystalline Ni-Rh alloys were prepared by arc melting the desired stoichiometric compositions of high-purity elements Ni and Rh in argon atmosphere. Atomic compositions of Ni and Rh in the alloys were independently checked by energy dispersive analysis of x-rays method. The alloys were further characterized by x-ray diffraction technique and found to have fcc structure for all compositions, and their lattice constants were found to be in agreement with those reported in the literature.[10]

Bulk magnetic susceptibility for Ni_xRh_{1-x} in the composition range $0.09 \leq x \leq 0.6$ was measured from 77 to 300 K in a magnetic field of 6 kG using a Faraday balance. The measurements were extended down to 5 K for $Ni_{0.6}Rh_{0.4}$ alloy. Figure 1 shows the inverse susceptibility $(1/\chi)$ as a function of temperature for all compositions after correcting for the Rh background, along with the $\chi(T)$ data for $Ni_{0.6}Rh_{0.4}$. None of the alloys studied showed magnetic ordering in the measured temperature range.

Microscopic studies on the magnetic behavior of Rh in Ni-Rh alloys were carried out by measuring local susceptibility of ^{100}Rh produced during the electron capture (EC) decay of ^{100}Pd. The parent ^{100}Pd (half-life=3.6 days) was produced by the heavy-ion reaction ^{89}Y (^{16}O,$p4n$) using a 95-MeV ^{16}O beam provided by the Pelletron Accelerator facility at TIFR, Bombay, and were recoil implanted into thin foils (typically 5 mg/cm^2) of Ni-Rh alloys. The concentration of ^{100}Pd in Ni-Rh alloys was typically less than 1 ppm.

TDPAC method. In the perturbed angular correlations (TDPAC) method, a parent isotope is introduced into the sample system. The required γ-γ cascade is populated by a preceding decay (either β or EC decay) from the parent isotope. The daughter nucleus, initially formed in an excited state I_i, decays to ground state I_f by successive emission of two γ rays via an intermediate state I having a lifetime τ. The detection of the first γ ray in a fixed direction k_1 leads to a selection of an ensemble of aligned nuclei in the intermediate state I. The second γ ray, emitted in a direction k_2, will have an anisotropic distribution of intensity with respect to k_1. In the presence of external magnetic fields, the nuclear spin I precesses with a Larmor frequency ω_L resulting in a time-dependent variation of the γ-ray anisotropy. By detecting these time modulations of the anisotropy the perturbing magnetic-field strength experienced by the nucleus can be extracted.[11]

In the present measurement we have used the 75 keV, $I=2^+$ level in ^{100}Rh ($T_{1/2}=235$ ns and $g_N=2.15$) as the nuclear probe for the detection of magnetic interaction. The magnetic response of Rh was measured in the range 25–700 K in an external magnetic field of 11 kG. Time spectra were recorded using three NaI(Tl) detectors placed in the ($\pm 135°$) geometry. The normalized ratio functions

$$R(t)=\frac{N(135°,t)-N(-135°,t)}{N(135°,t)+N(-135°,t)} \quad (1)$$

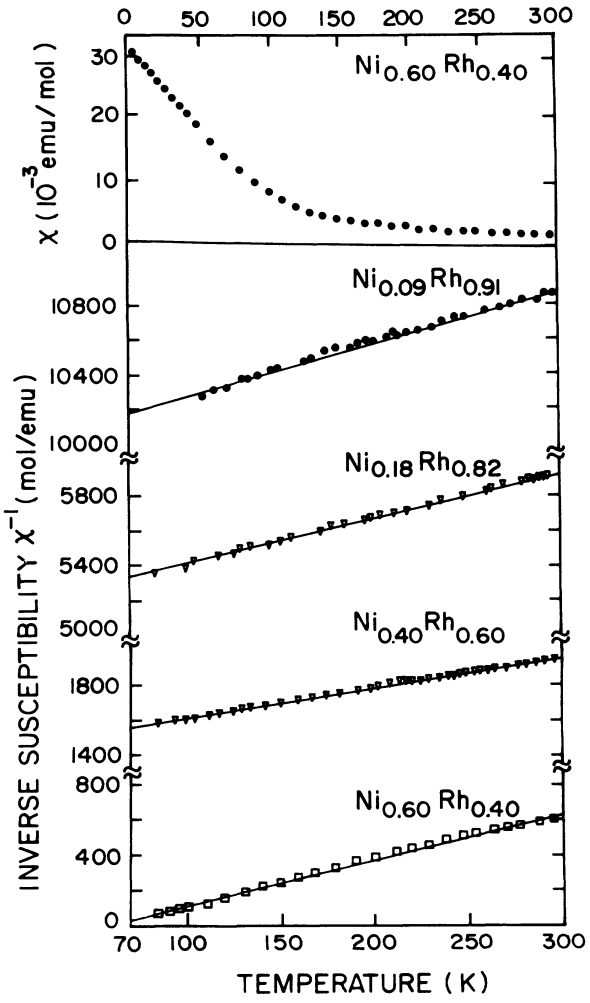

FIG. 1. Temperature dependence of inverse bulk magnetic susceptibility, χ^{-1}, for several Ni-Rh alloys measured in a field of 6 kG. The top panel shows the χ vs T plot for $Ni_{0.6}Rh_{0.4}$ measured in a field of 15 kG.

formed from the data were fitted to the function

$$R(t)=(3/4)A_2\sin(2\omega_L t-\phi) \quad (2)$$

to extract the Larmor frequency ω_L. Figures 2(a) and 2(b) show typical spin-rotation spectra $R(t)$ for different Ni-Rh alloys. From the measured value of $\omega_L = \hbar^{-1} g_N \mu_N B_{\text{ext}} \beta$, the paramagnetic enhancement factor β was estimated. The quantity $\beta-1$ gives a measure of the local susceptibility at the ^{100}Rh probe site, which in turn yields information on its magnetic behavior.[8] Figure 3 displays the temperature dependence of the Rh local susceptibility in different Ni-Rh alloys. Here, $\beta=1(\pm 0.02)$ is the parameter used to identify nonmagnetic behavior, e.g., Rh in Rh, with negligible spin polarization at the probe atom, while $\beta<1$ is taken to signify

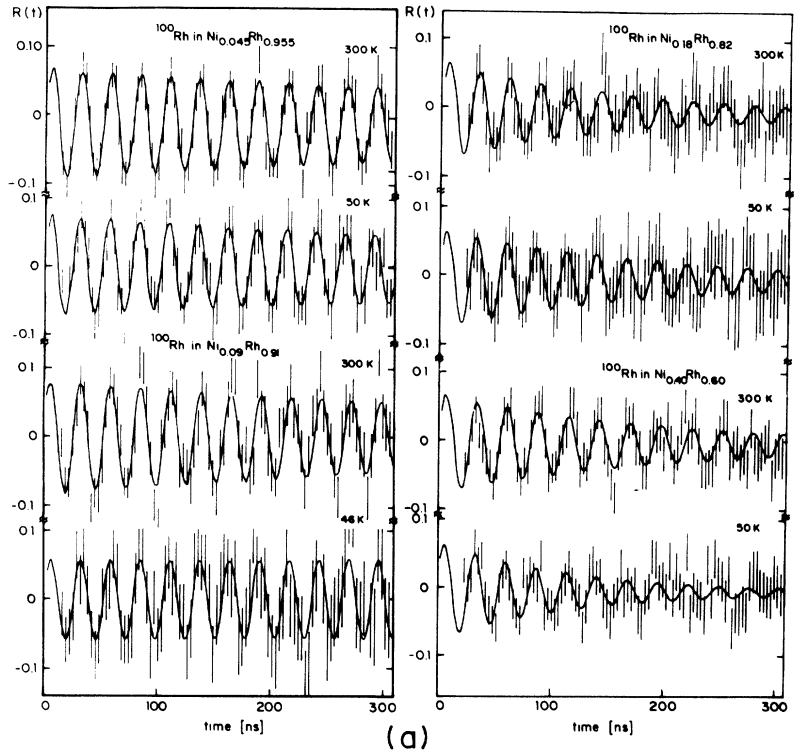

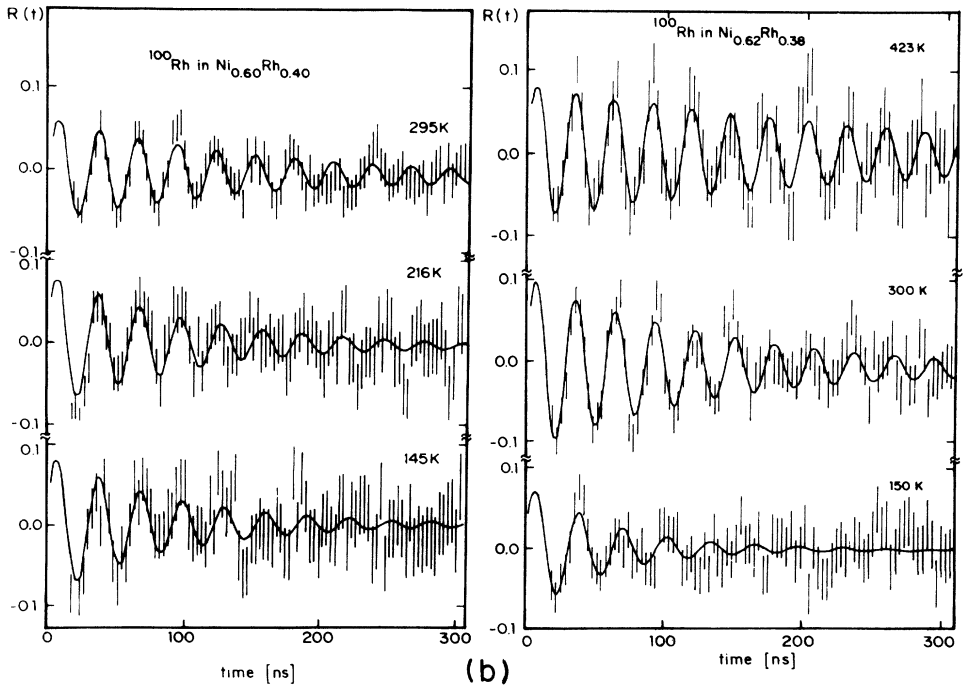

FIG. 2. Spin rotation spectra, $R(t)$ for Ni-Rh alloys of various concentrations and at different temperatures measured in a field of 11 kG.

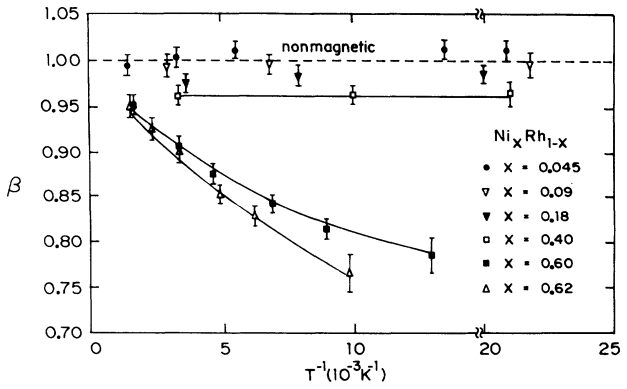

FIG. 3. The parameter β as a function of inverse temperature for various Ni-Rh alloys.

the existence of large spin susceptibility arising from the polarization of the core and/or the conduction electrons. In systems where the probe atoms acquire a magnetic moment the measured local susceptibility data show Curie-Weiss–type temperature dependence;[8] $\beta(T)-1=C/(T+T^*)$, where C is the Curie constant and T^* is a characteristic temperature analogous to the paramagnetic Curie-Weiss temperature, known from the bulk susceptibility data.

III. EXPERIMENTAL RESULTS

A. Bulk magnetization

Bulk magnetic susceptibility data taken in a field of 6 kG for all alloy compositions in the series Ni_xRh_{1-x} (see Fig. 1) show paramagnetic behavior down to 77 K. The data were fitted to a Curie-Weiss law $\chi=C/(T-\theta_P)$ to extract the effective paramagnetic moment μ_{eff} per unit cell and the Curie-Weiss temperature θ_P. The results for the various parameters are summarized in Table I. Our results for C and θ_P are in good agreement with the corresponding values we could extract from the susceptibility data reported by Cottet *et al.*[12] An initial analysis of the data assuming that Rh atoms are nonmagnetic and the entire temperature-dependent magnetic susceptibility arises from magnetic moments on Ni atoms only results in unrealistically high magnetic moments on the Ni atoms, $\mu_{\text{Ni}} \gg 1$, especially in the Rh-rich alloys. Since the magnetic moment on Ni in metallic systems is found to be between $0.6-1.0\mu_B$[13], we are led to acknowledge that the Rh atoms also acquire substantial spin polarization. Using reasonable values $\mu_{\text{Ni}}=0.4\mu_B$ for $x \leq 0.4$ and $\mu_{\text{Ni}}=0.6\mu_B$ for $x \sim 0.6$, in conformity with our theoretical calculations (see Sec. IV), we estimate the magnetic moments μ_{Rh} on the Rh atoms, which are listed in Table I. We find that for $0.9 < x < 0.6$, both Ni and Rh atoms are magnetic. The values for μ_{Rh} are found to be $0.4\mu_B$ for $Ni_{0.09}Rh_{0.91}$, which decrease to $0.29\mu_B$ for $Ni_{0.6}Rh_{0.4}$.

Secondly, the Curie-Weiss temperature θ_P derived from the susceptibility data show strong dependence with the Ni concentration, varying from a quite high ~ -3000 K for $x=0.09$ to 42 K for $x=0.6$. It is interesting to note that θ_P changes sign when x increase from 0.4 to 0.6.

B. TDPAC measurement—^{100}Rh local susceptibility

For all Ni-Rh alloys, the $R(t)$ spectra [see Fig. 2(a) and Fig. 2(b)] show high anisotropy and well-defined oscillations at all temperatures indicating that most of the recoil implanted ^{100}Pd ions come to rest at unique lattice sites in the host. Most probably, the ^{100}Pd ions occupy Rh sites in all the Ni-Rh alloys. In the random alloys under investigation, Rh atoms are expected to have a distribution in the near-neighbor (NN) atomic configuration. However, the limited accuracy of our measurements does not permit observation of distinctly resolved frequencies corresponding to different near-neighbor configurations. The local susceptibility $\beta-1$ derived from the observed Larmor frequency ω_L, therefore, corresponds to an average value over all possible NN configurations.

The magnetic response of ^{100}Rh in Ni_xRh_{1-x} alloys with low Ni concentrations, $x < 0.4$, show temperature independent local susceptibility with $\beta(T)$ values close to unity. For $Ni_{0.4}Rh_{0.6}$ the β value at room temperature was obtained to be 0.95, which was also found to have little variation with temperature, indicating enhanced spin susceptibility at the Rh probe site. On further increasing the Ni concentration, the $\beta(T)$ data was found to show large deviations from the nonmagnetic $\beta=1$ behavior along with strong temperature dependence. We like to note that our Rh local susceptibility values in the Ni-rich alloys, i.e., $x \geq 0.6$, are slightly higher compared to those reported from the NMR measurements.[12] The measured $\beta(T)$ results for Rh in $Ni_{0.6}Rh_{0.4}$ and $Ni_{0.62}Rh_{0.38}$ could

TABLE I. Summary of Curie-Weiss fit parameters to the bulk susceptibility data in Ni_xRh_{1-x}. x is the composition, C is the Curie-constant, θ_P is the paramagnetic Curie-Weiss temperature, μ_{eff} is extracted effective magnetic moment per unit cell, and μ_{Rh} is the magnetic moment on a Rh atom.

Composition x	C (emu K/mol)	θ_P (K)	μ_{eff}[a] (μ_B)	μ_{Rh} (μ_B)	μ_{eff}[b] (μ_B)
0.09	0.33	−3227	1.63	0.41	1.10
0.18	0.39	−1331	1.76	0.45	1.65
0.40	0.60	−870	2.03	0.58	2.40
0.60	0.41	42	1.90	0.29	2.93

[a]From bulk susceptibility data.
[b]Calculated.

be fitted to a Curie-Weiss law (see above). The derived C and T^* values come out to be -37 K, 100 K, and -39 K, 63 K, respectively (also see Table II). The high negative value of the Curie constant C for ^{100}Rh in Ni_xRh_{1-x} alloys is consistent with the presence of large spin polarization around the probe Rh atom. Considering the Rh magnetic behavior arrived at from the bulk susceptibility data and the electronic structure calculations (see below) the temperature independent $\beta(T)$ values observed in the low-Ni concentration alloys ($x \leq 0.4$) can be consistent with high-spin-fluctuation temperatures, $T^* \sim 10^3$ K for the Rh moment.

We also estimate the magnetic moment corresponding to the total spin polarization seen by the Rh probe in Ni-Rh system. The Curie constant obtained from the Rh local susceptibility is related to net spin polarization and hence magnetic moment seen by the Rh atom via the relation $C = 2\mu_B(S_t+1)B(0)/3k_B$ where $B(0)$ is the contact hyperfine field at the Rh nucleus and S_t is the sum of the spin at the probe atom, S_{probe}, and the spin polarization S_{host} coming from the surrounding atoms. The core polarization hyperfine field $B(0)$ for most $4d$ ions have been estimated and also experimentally measured[14] to be $-350kG/\mu_B$. Using $B(0) = -140$ kG corresponding to a spin $S_{\text{probe}} = 0.2$ at the probe atom, consistent with the magnetic moment values of Rh found from our bulk susceptibility data, we estimate S_t and the total magnetic moment $\mu_{\text{tot}} = 2S_t$ seen by the probe Rh atoms in different Ni-Rh alloys. The values are listed in Table II. The derived values are quite high, $\mu_{\text{tot}} \sim 10\mu_B$, even higher than those observed for some $4d$ ions in transition metals, e.g., Rh and Ru in Pd.[2,3] The high value of the total spin and Rh magnetic moment for $x_{\text{Ni}} \sim x_{\text{crit}}$ suggests that even on the paramagnetic side of x_{crit}, Rh atoms acquire significant spin polarization present on the surrounding Ni atoms. We like to note that if we use $B(0) \sim -190$ kG/μ_B, as suggested by Narath and Weaver,[6] our results for S_t and μ_{tot} would come out to be even higher. This variation in $B(0)$ does not change the essential conclusions we have drawn below.

IV. THEORETICAL CALCULATIONS AND RESULTS

In conjunction with the experimental measurements, we also carried out an illustrative theoretical study of the local magnetic behavior of Ni and Rh atoms in Ni-Rh alloys as a function of the number and position of Ni and Rh atoms in their immediate environment. To this end, we perform electronic-structure calculations via the *ab initio* self-consistent-field LCAO-MO method within the local-spin-density approximation[15] using atomic clusters to simulate the bulk. Since this technique has been severally described[16] in detail before, only those aspects relevant to the present calculation and subsequent analysis of results are given here. Essentially, typical 19 atom clusters $M_1M_{12}M_6$ ($M \equiv$ Ni or Rh) comprising two full coordination shells of atoms in fcc lattice geometry around a central (probe) atom M_1 are chosen for explicit treatment of their wave functions and eigenvalues. Different environments for the central probe atom (M_1) are simulated by placing a varying number of Ni and Rh atoms in the coordination shells. As a binomial expansion in the concentration x shows, they reflect actual configurations occurring in a Ni_xRh_{1-x} alloy, their relative abundances changing with x. Previously, calculations[17] of the paramagnetic spin susceptibility of Ni-Rh alloys as a function of concentration x within the coherent potential approximation have been reported and have alluded to the dependence of atomic moments on the local NN environment. In the present work, the approach is reversed: our accent is on considering specific NN configurations directly and attempting to construct an effective moment to compare with experimental susceptibilities.

TABLE II. Summary of derived parameters from the Curie-Weiss fit to the ^{100}Rh local susceptibility in Ni_xRh_{1-x}. C is the Curie-constant, T is the characteristic temperature, S_t is the total spin, and μ_{tot} is the extracted total moment per Rh atom.

Composition x	C (K)	T^* (K)	S_t	μ_{tot} (μ_B)
0.60	$-37(1)$	100(15)	4.9	9.8
0.62	$-39(1)$	63(15)	5.2	10.4

The one-electron Hamiltonian for a cluster, as a functional of the electron charge density $\rho(\mathbf{r})$, is given in atomic units by

$$H_\sigma(\mathbf{r}) = (-1/2)\nabla^2 + V_C(\rho) + V_\sigma^{XC}(\rho_\sigma) , \tag{3}$$

where $V_C(\rho)$ is the conventional electron-electron plus electron-nucleus Coulomb potential and $V_\sigma^{XC}(\rho_\sigma)$ is a local spin(σ)-dependent exchange correlation potential of the form derived by von Barth and Hedin.[15] Molecular-orbital eigenfunctions $\phi_{i\sigma}(\mathbf{r})$ of the above Hamiltonian are expanded on a basis of numerical atomic orbitals: $3d, 4s, 4p$ on Ni atoms and $4d, 5s, 5p$ on Rh atoms; the deeper-lying atomic orbitals in each case are treated as nonvariational. The resulting variational secular equation is finally solved iteratively to self-consistency using Hamiltonian and overlap matrix elements determined by three-dimensional numerical integration on a pseudorandom grid, except for a systematic polynomial integration within a sphere of radius 2 a.u. around the M_1 atom, expressly to ensure precision in the hyperfine field. From the resulting one-electron eigenvalues, eigenfunctions, and occupation indices $f_{i\sigma}$, the charge and spin magnetization densities,

$$\rho_\sigma(\mathbf{r}) = \sum_i f_{i\sigma} |\phi_{i\sigma}(\mathbf{r})|^2 , \tag{4a}$$

$$\delta\rho(\mathbf{r}) = \rho_\uparrow(\mathbf{r}) - \rho_\downarrow(\mathbf{r}) , \tag{4b}$$

are constructed and their Mulliken population analysis yields the site-specific local spin density of states (LDOS).

The main contribution to the hyperfine field H_{hf} seen by a magnetic or nonmagnetic probe atom comes from the Fermi contact interaction, which can be calculated in terms of the spin magnetization density at the nucleus,

$$H_{\rm hf} \approx H_c = \frac{8\pi}{3}\frac{g_s}{2}\mu_B[\rho_\uparrow(0)-\rho_\downarrow(0)]$$
$$= 524.2[\delta\rho(0)]_{\rm a.u.}\ \text{kG} . \quad (5)$$

To this first approximation, the orbital contribution to $H_{\rm hf}$ is neglected because of quenching of the orbital angular momentum. We can further single out two contributions to $H_{\rm hf}$ for separate treatment. A core-polarization contact field $H_{\rm hf}^{\rm core}$ results from the polarization of core-s electrons due to the spin imbalance in the d shell. From the states close to the Fermi energy, the polarized conduction band s electrons associated with the impurity and the tails of the orbitals on the surrounding host atoms contacting the probe nucleus together give a "band" contribution $H_{\rm hf}^{\rm val}$. This latter is a direct by-product of our self-consistent calculations.

The present approach is particularly suited for looking at local properties, determined by overlap and bonding within the immediate atomic environment, rather than band effects. Previous work has shown that, considering the size of the representative cluster, the charge and spin density in the central region of the cluster, i.e., that associated with the M_1 atom, is adequately bulklike; however, the results for the two outer sets of atoms, M_{12} and M_6, are subject to "surface" effects deriving from incomplete coordination and, hence, reduced orbital overlaps and hybridization. These include an upward shift in energy levels, narrower LDOS, and larger orbital local moments.

Table III is a summary of our calculated results for the valence orbital Mulliken population charges and local moments, the density of states at the Fermi energy E_F, and hyperfine levels at a Ni atom site in Ni-Rh alloys. Table IV is, likewise, a similarly presented collation of our results for a central probe Rh atom. The first four columns in each table give details of the clusters used to represent alloys of varying concentrations. The description of the clusters indicates the inequivalent sets of Ni and Rh atoms in the first- and second-neighbor shells, which are treated separately in the variational procedure. As we move down the rows, the number $\bar{n}$ of Ni nearest-neighbors (NN) increases in steps of 2. The cluster symmetry is intended to indicate the particular placement of the coordinating atoms. Only a few highly symmetric configurations of the total number of $\sum_r^{12} {}^{12}C_r = 4096$ possibilities have been studied at each $\bar{n}$; nevertheless, they are adequate for the purpose of exhibiting trends with $\bar{n}$ and typical values of the parameters considered.

The host lattices and the alloy systems in the middle four rows ($\bar{n}=4$ to 8) have undistorted fcc geometry with NN distance $d = a/\sqrt{2}$. The lattice constants a for the alloy systems are obtained by interpolating between the a values for the host elements, using the host bulk modulii and $\bar{n}$. However, for the case of isolated and decorated impurities, we find it important to allow for local relaxation of only the first-neighbor atoms in adjustment to the different sizes of the Ni and Rh atoms [r_a(Ni)=1.24 Å, r_a(Rh)=1.34 Å]. Displacements of further neighbor atoms are expected to be an order of magnitude less, and so they are left undisturbed.

For the host Ni and for the host Rh, our results for the charge density, the local density of states and the local moments are in good agreement with the conventional local-density band-structure calculations by Moruzzi, Janak, and Williams,[13] which give $N_F=1.69$ states/eV and $\mu=0.58\mu_B$ per Ni atom, $N_F=1.35$ states/eV per atom and $\mu=0\mu_B$ per Rh atom.

We find an isolated Ni impurity in Rh ($\bar{n}=0$) to be nonmagnetic, in agreement with the experimental results,[5,7] but only after allowing for the inward relaxation

TABLE III. Calculated parameter values for Ni atoms in Ni-Rh alloys, with nearest-neighbor Ni atom coordination number ($\bar{n}$) varying in steps of 2 from 0 to 12: valence orbital Mulliken population charges ($n_\uparrow+n_\downarrow$) and magnetic moments ($n_\uparrow-n_\downarrow$) in μ_B, net ionicity (Q) and net local moment μ, local density of states at $E_F(N_F)$ and contact hyperfine fields ($H_{\rm hf}$) with core and valence contributions. Details of the molecular clusters used in the calculations are also given.

Cluster employed	Cluster symmetry	No. of NN Ni ($\bar{n}$)	Cluster geometry	$(n_\uparrow+n_\downarrow)$(Ni$_1$) $(n_\uparrow-n_\downarrow)$(Ni$_1$) 3$d$	4s	4p	Q(Ni$_1$) μ(Ni$_1$) (e^-,μ_B)	N_F(Ni$_1$) states/eV	$H_{\rm hf}^{\rm core}+H_{\rm hf}^{\rm val}=H_{\rm hf}$(Ni$_1$) (kG)
$Ni_1Rh_{12}Rh_6$	O_h	0	$a=3.80$ Å	8.94	0.43	1.26	−0.63	2.03	0
			$d=2.61$ Å	0.00	−0.01	0.01	0.00		
$Ni_1(Ni_2Rh_8Rh_2)$	D_{2h}	2	$a=3.80$ Å	8.93	0.45	1.29	−0.67	1.91	−37−23
(Rh_4Rh_2)			$d=2.61$ Å	0.37	−0.01	0.01	0.37		=−60
$Ni_1(Ni_4Rh_8)$	D_{4h}	4	$a=3.71$ Å	8.90	0.48	1.40	−0.78	1.70	−43−39
(Ni_2Rh_4)			$d=2.62$ Å	0.43	−0.02	0.01	0.42		=−82
$Ni_1(Ni_6Rh_6)Ni_6$	D_{3d}	6	$a=3.67$ Å	8.96	0.45	1.23	−0.64	1.70	−38−44
[planar NN Ni_6]			$d-2.59$ Å	0.38	−0.02	−0.03	0.33		=−82
$Ni_1(Ni_6Rh_6)Rh_6$	D_{3d}	6	$a=3.67$ Å	8.92	0.39	1.13	−0.44	1.52	−74−37
[3D NN Ni_6]			$d=2.59$ Å	0.74	−0.015	−0.025	0.70		=−111
$Ni_1(Ni_8Rh_4)$	D_{4h}	8	$a=3.62$ Å	8.88	0.49	1.28	−0.65	1.60	−76−35
(Ni_4Rh_2)			$d=2.56$ Å	0.76	−0.015	−0.005	0.74		=−111
$Ni_1(Ni_2Ni_8Rh_2)$	D_{2h}	10	$a=3.52$ Å	8.92	0.44	1.56	−0.92	1.76	−59−55
(Ni_4Ni_2)			$d=2.51$ Å	0.59	−0.02	−0.05	0.52		=−114
$Ni_1Ni_{12}Ni_6$	O_h	12	$a=3.52$ Å	8.94	0.40	1.16	−0.50	1.64	−58−62
			$d=2.49$ Å	0.58	−0.02	−0.02	0.54		=−120
									(expt. =−76)

TABLE IV. Calculated parameter values for Rh atoms in Ni-Rh alloys, with nearest-neighbor Ni atom coordination number ($\bar{n}$) varying in steps of 2 from 0 to 12: valence orbital Mulliken population charges ($n_\uparrow + n_\downarrow$) and magnetic moments ($n_\uparrow - n_\downarrow$) in μ_B, net ionicity (Q) and net local moment μ, local density of states at E_F(N_F) and contact hyperfine fields (H_{hf}) with core and valence contributions. Details of the molecular clusters used in the calculations are also given.

Cluster employed	Cluster symmetry	No. of NN Ni ($\bar{n}$)	Cluster geometry	$(n_\uparrow+n_\downarrow)(Rh_1)$ $(n_\uparrow-n_\downarrow)(Rh_1)$ 4*d*	5*s*	5*p*	$Q(Rh_1)$ $\mu(Rh_1)$ (e^-,μ_B)	$N_F(Rh_1)$ states/eV	$H_{hf}^{core}+H_{hf}^{val}$ $=H_{hf}(Rh_1)$ (kG)
$Rh_1Rh_{12}Rh_6$	O_h	0	$a=3.80$ Å	8.05	0.33	1.03	−0.41	1.44	0
			$d=2.69$ Å	0.00	0.00	0.00	0.00		
$Rh_1(Ni_2Rh_8Rh_2)$	D_{2h}	2	$a=3.80$ Å	8.09	0.30	0.93	−0.32	1.47	−118−18
(Rh_4Rh_2)			$d=2.61$ Å	0.55	−0.005	0.035	0.58		=−136
$Rh_1(Ni_4Rh_8)$	D_{4h}	4	$a=3.71$ Å	8.03	0.39	1.28	−0.70	1.47	−108−31
(Ni_2Rh_4)			$d=2.62$ Å	0.50	−0.005	0.05	0.545		=−139
$Rh_1(Ni_6Rh_6)Ni_6$	D_{3d}	6	$a=3.67$ Å	8.16	0.28	0.82	−0.26	1.23	−127−53
[planar NN Ni_6]			$d=2.59$ Å	0.59	−0.015	−0.005	0.57		=−180
$Rh_1(Ni_6Rh_6)Rh_6$	D_{3d}	6	$a=3.67$ Å	8.09	0.23	0.76	−0.08	1.15	−204−13
[3D NN Ni_6]			$d=2.59$ Å	0.95	−0.01	0.00	0.94		=−217
$Rh_1(Ni_8Rh_4)$	D_{4h}	8	$a=3.62$ Å	8.03	0.37	0.91	−0.31	1.38	−187−33
(Ni_4Rh_2)			$d=2.56$ Å	0.87	−0.02	0.03	0.88		=−220
$Rh_1(Ni_2Ni_8Rh_2)$	D_{2h}	10	$a=3.52$ Å	8.09	0.27	1.39	−0.75	1.41	−174−72
(Ni_4Ni_2)			$d=2.51$ Å	0.81	−0.01	−0.01	0.79		=−246
$Rh_1Ni_{12}Ni_6$	O_h	12	$a=3.52$ Å	8.14	0.24	0.68	−0.06	1.30	−172−77
			$d=2.51$ Å	0.80	−0.015	0.005	0.79		=−249
									(expt. =−225)

of the NN Rh atoms from their nominal unrelaxed distance $d=2.69$ Å in the host to $d=2.61$ Å. This distance is just 0.03 Å larger than the sum of atomic radii of Ni and Rh. In the absence of an energy minimization procedure to determine the exact NN distance, we can only suggest that d lies between 2.58 and 2.61 Å. Within this 0.08 Å relaxation, the local d-moment on the central Ni is quenched from $0.62\mu_B$ to $0\mu_B$. A similarly small local relaxation, arising from size mismatch, has been shown to account for the nonmagnetic behavior of isolated Fe atoms in Al.[18] An isolated Rh impurity in Ni ($\bar{n}=12$) exhibits a substantial local d moment of $0.80\mu_B$. This value is larger than the $0.59\mu_B$ value calculated by Zeller,[19] which would suggest that the Rh atom simply acquires the polarization of the surrounding Ni atoms. A Rh atom in Ni is, however, not isoelectronic to a Ni atom, so a different μ value is plausible.

At the high $\bar{n}$ end of the tables ($\bar{n}\geq 6$), the NN Ni atom coordination mostly reflects situations within Ni_xRh_{1-x} alloys in the ordered ferromagnetic regime ($1>x>0.63$). Here, the Rh d moment is consistently $\gtrsim 0.8\mu_B$ and increases slightly as the NN Ni atoms decrease and move further away. The d moment on the Ni atoms also increases gradually with decreasing $\bar{n}$, from its bulk value of $0.58\mu_B$ to a maximum of $\sim 0.75\mu_B$. The low $\bar{n}$ end of the tables ($\bar{n}\leq 6$) is representative of Ni_xRh_{1-x} alloys in the wide paramagnetic region ($x<0.63$). Here, the Ni d moment quickly saturates with NN Ni decoration to $\sim 0.4\mu_B$, while the Rh d moment remains at $0.5-0.6\mu_B$. The variation in the calculated μ values for small changes in NN distances up to 0.03 Å do not exceed $\pm 0.05\mu_B$. The striking feature is that atomic spin moments on both Ni and Rh atoms persist for all $\bar{n}\geq 2$ at least and hence, by implication, throughout most of the Ni concentration range.

Clearly, too, the strength of the local moment peaks for certain NN configurations near $\bar{n}=6$. The underlying mechanism of moment formation has also a topological dependence, as is revealed by the two $\bar{n}=6$ clusters studied. Atoms with a three-dimensional (3D) NN Ni atom arrangement typically exhibit the higher moment values; when the decoration of NN Ni atoms is planar or linear, the lower μ values are obtained. This geometrical influence is expected to show up for other NN arrangements, not studied here, in the middle range of $\bar{n}$; for larger $\bar{n}$, of course, nearly all the arrangements tend to be three dimensional. The dominance of the latter, more spherically symmetrical, type of configurations over the lower-dimensional ones becomes significant beyond a threshold value $\bar{n}\sim 6$. The ponderance of these NN Ni atom configurations in Ni-rich regions coincides with the sharp rise observed in the bulk susceptibility for $x>0.5$. Thus, for both Ni and Rh atoms we obtain two characteristic signatures each for the spin moments, with comparatively only slight variations in the magnitude of each. For less symmetric NN atom arrangements than the ones considered here, realistically speaking we can only say that the arrangement-geometry criterion explored above must still hold, so that two sets of moment values would still be obtained.

Note also, in all cases, the small, but significant, moments on the conduction band s orbitals, antiferromagnetically aligned relative to the d moments. Since this is also true of the valence orbitals on the surrounding atoms, we suggest that this d-s hybridization is the source of the magnetic screening in the system. It is to be pointed out here that both the s and p moments calculated are overestimated, since these extended orbitals are

most affected by the spurious polarization of the adjoining surface shells of cluster atoms, given the size of the clusters. Consequently, the contribution $H_{\rm hf}^{\rm val}$ is also exaggerated.

Blügel *et al.*[20] have shown that inclusion of relativistic effects does not have much effect on the magnitudes of the local moments calculated, but is essential for obtaining a proper core contribution $H_{\rm hf}^{\rm core}$ to the hyperfine field, arising from the polarization of core-*s* electrons due to the spin imbalance in the outermost *d* shell. Following their local-density calculations within a semirelativistic approximation for 3*d* and 4*d* impurities in Ni, we use 100 kG/*d* moment for Ni and 215 kG/*d* moment for Rh for the core hyperfine field $H_{\rm hf}^{\rm core}$, to use along with our nonrelativistic calculated moments. These core and valence contributions and their sum $H_{\rm hf}$ are given in the last columns of Tables III and IV. Even so, two characteristic sets of values for the Rh hyperfine field are obtained, $|H_{\rm hf}({\rm Rh})| \gtrsim 200$ kG and $|H_{\rm hf}({\rm Rh})| \lesssim 150$ kG, reflecting the two distinctive sets of moment values they are derived from. A similar scenario is also valid for the hyperfine fields on Ni.

The panel of Figs. 4(a)–4(c) for the LDOS shows the development of the local moments at Ni and Rh sites having $\bar{n}=4$, and for a hypothetical $Ni_{1/3}Rh_{2/3}$ alloy made up of only such Ni and Rh atoms; in a sense, the latter may be taken as a typical alloy of the paramagnetic region. Figures 5(a)–5(c) is the corresponding analogue for $\bar{n}=8$: the LDOS for Ni and Rh sites and for a $Ni_{2/3}Rh_{1/3}$ alloy constructed from them, a prototype

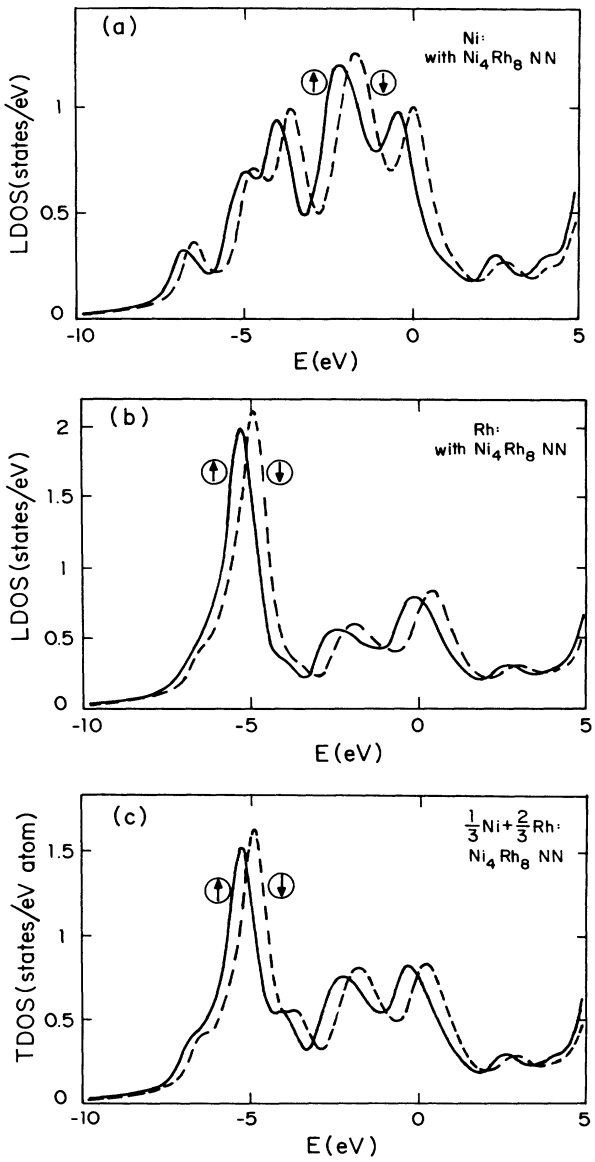

FIG. 4. Local density of states for (a) Ni and (b) Rh atoms with $\bar{n}=4$. (c) Total density of states per atom for a $Ni_{1/3}Rh_{2/3}$ alloy, obtained as a concentration-weighted sum of $(a)+(b)$. The arrows refer to spin-up and spin-down components, respectively.

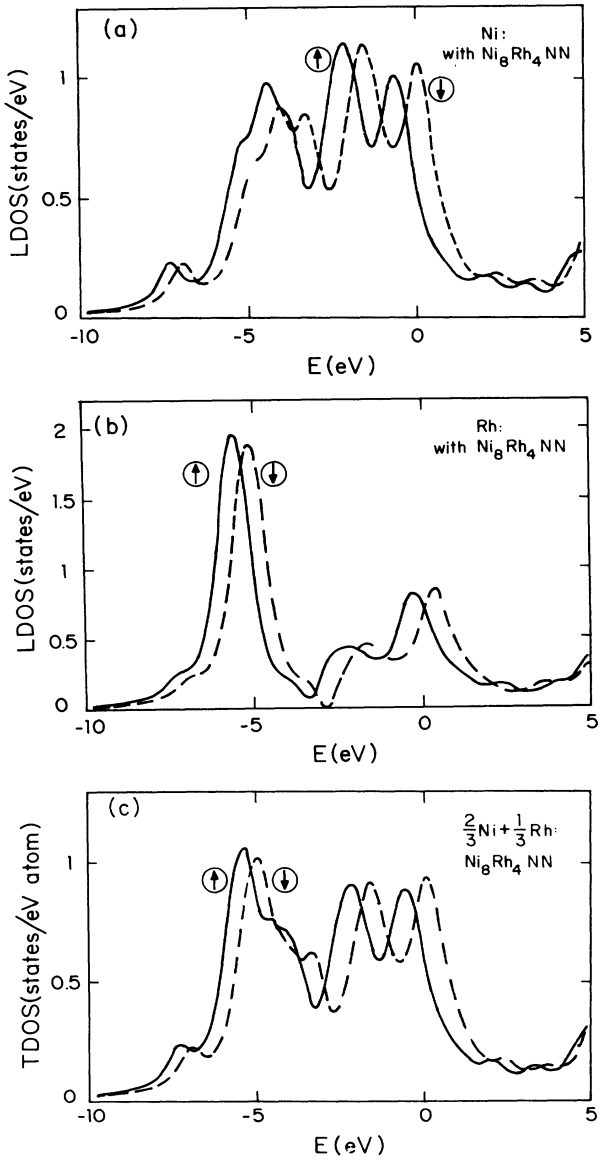

FIG. 5. Local density of states for (a) Ni and (b) Rh atoms with $\bar{n}=8$. (c) Total density of states per atom for a $Ni_{2/3}Rh_{1/3}$ alloy, obtained as a concentration-weighted sum of $(a)+(b)$. The arrows refer to spin-up and spin-down components, respectively.

"ferromagnetic" alloy. For Rh, we find bonding and antibonding orbitals ~ 5 eV on either side of E_F. The formation of a local moment on Rh is related to the fact that of the nonbonding orbitals straddling E_F, the majority (spin-up) orbitals are increasingly pulled below E_F as $\bar{n}$ increases; the resulting exchange splittings near E_F are 0.55 eV for $\bar{n}=4$, 0.65 eV for $\bar{n}=8$ and 0.70 eV for $\bar{n}=12$. For Ni, the peak of the nonbonding orbitals remains pinned to E_F, while the corresponding exchange splittings near E_F are 0.45 eV for $\bar{n}=4$ and 0.7 eV for $\bar{n}=8$.

For both Ni and Rh atoms, N_F, the density of states at E_F, is almost wholly of d character. Its general trend is a decrease with increasing $\bar{n}$, more pronounced for Ni (20% across the table) and slighter for Rh ($<10\%$), punctuated by an anomalous dip near $\bar{n}=6$, which reflects the transition to more spherically symmetric arrangement of Ni atoms and coincides with the peak in $\mu(\bar{n})$ for both types of atoms.

To correlate the moments calculated above for different $\bar{n}$ with the measured bulk and local susceptibility data for different alloys Ni_xRh_{1-x}, we interpolate on the moments calculated for even $\bar{n}$ to obtain those for odd $\bar{n}$ values, and assume a binomial distribution in $\bar{n}$ for NN Ni and Rh atoms at each concentration x. This procedure yields an effective local moment μ_{eff} per unit cell as a function of x, values of which are given in the last column of Table I for comparison with the μ_{eff} extracted from the bulk susceptibility. We see that the calculated values increase more sharply and continuously with x, and have a higher peak value $\mu=2.95\mu_B$ at $x\sim 2/3$; beyond this, they fall off again to the bulk Ni moment value, $\mu=2.32\mu_B$, thereby mimicking the experimental trend. However, given the few and restricted geometries for which the calculations are carried out, it is not surprising that the detailed structure of the trend, especially the narrow peak near x_{crit}, is not reproduced.

V. DISCUSSION

The bulk susceptibility as well as the ^{100}Rh local susceptibility results presented above show the existence of large stable magnetic moments on Rh in Ni_xRh_{1-x} alloys with $x=0.60$ and 0.62. Keeping in mind that the bulk susceptibility data in low Ni concentration alloys as well as the theoretical results reflect the presence of magnetic moments on the Rh atoms, the observed temperature independent local susceptibility data with $\beta(T)\sim 1$ for ^{100}Rh in these alloys can be reconciled with high spin-fluctuation temperatures, which are estimated to be $>10^3$ K for Rh in Ni_xRh_{1-x} for $x\lesssim 0.4$. The paramagnetic Curie-Weiss temperatures θ_P obtained from the bulk susceptibility data, which can also be used to scale the spin-fluctuation temperature, come out to be very high in this concentration range (see Table I), implying unstable moment for Ni as well as Rh. Also, in this regime the calculations indicate antiferromagnetic d-s coupling, which probably is strong enough to screen the moments. Further, the antiferromagnetic nature of the exchange interaction is also reflected in the negative sign of θ_P in these alloys. It is interesting to note that for $x\sim x_{\text{crit}}=0.63$ the magnitude of θ_P values are found to decrease quite sharply with a concomitant change in sign, suggesting that the coupling between the various magnetic moments is predominantly ferromagnetic in nature. This is also supported by the fact that long-range ferromagnetic ordering sets in the alloy system beyond $x=0.63$ indicating increasingly stable moments on Ni and perhaps on Rh as well. Comparing the bulk and the local susceptibility data, we feel that the presence of stable Ni magnetic moment in the vicinity of the Rh probe atom and the ferromagnetic nature of the interatomic exchange coupling makes the Rh moment quite stable leading to the observation of a Curie-Weiss like $\beta(T)$.

The derived values of S_t and μ_{tot} for $x\sim x_{\text{crit}}$ are quite high, even higher than those observed for some $4d$ ions in transition metals, e.g., Rh and Ru in Pd.[2,3] The high value of the total spin and the Rh magnetic moment for $x\sim x_{\text{crit}}$ suggests that even in the paramagnetic side of x_{crit}, Rh atoms acquire significant spin polarization present in the surrounding Ni atoms.

We now attempt to correlate the magnetic response of Rh in Ni_xRh_{1-x} alloys across the concentration range to near-neighbor atomic environment. The fcc lattice of a Ni-Rh alloy with a coordination number of 12 is randomly occupied by both Ni and Rh atoms resulting into a distribution of atoms in the near-neighbor atomic shells. We consider only the nearest-neighbor (NN) atomic shell, since further shell effects are negligible in our local susceptibility measurements. The probability distribution of Rh having different numbers of Ni atoms in the NN shell along with the observed Rh local susceptibility data indicates that Rh acquire large spin polarization beyond a threshold value of $\bar{n}\sim 6$. Similar results have also been reported for Rh in Fe-Rh systems, where Rh is suggested to acquire magnetic moment when surrounded by four or more Fe atoms in the NN shell.[21]

In summary, we have made a detailed investigation of the magnetic behavior of Rh in Ni_xRh_{1-x} alloys for several compositions $0.045<x<0.62$ below the critical composition $x=0.63$ for appearance of ferromagnetism by measuring local susceptibility at ^{100}Rh and the bulk magnetization. Complementing the experimental studies we have also performed local-spin-density calculations for atomic spin moments on Ni and Rh atoms having different NN configurations. For $x\lesssim 0.4$, Rh is found to have unstable magnetic moments with high spin-fluctuation temperatures ($T_{\text{SF}}\sim 10^3$ K). Near $x=0.63$ large spin polarization surrounding the Rh probe atoms result in the appearance of increasingly stable high Rh magnetic moment with $\mu_{\text{tot}}\sim 10\mu_B$. The increase in μ_{Ni} and μ_{Rh} is correlated with the growing number of three-dimensional and more spherically symmetric configurations of the NN Ni atoms when the number of Ni near neighbors exceeds a threshold value of ~ 6. Our experimental results as well as theoretical calculations show that Rh magnetic behavior is strongly influenced by the sign of the interatomic exchange interaction. In particular, the observed enhanced Rh magnetic response near $x\sim 0.6$ is attributed to the ferromagnetic d-d interaction between Rh and Ni atoms.

ACKNOWLEDGMENTS

We thank Ravi Kumar, V. Suryakamala, and the Pelletron Accelerator staff for their help during the experiment.

[1]For a review, see D. Riegel and K. D. Gross, Physica B **163**, 678 (1990).

[2]K. D. Gross, D. Riegel, and R. Zeller, Phys. Rev. Lett. **65**, 3044 (1990).

[3]S. Khatua, S. N. Mishra, S. H. Devare, and H. G. Devare, Phys. Rev. Lett. **68**, 1038 (1992).

[4]M. R. Press, S. N. Mishra, S. H. Devare, and H. G. Devare, Phys. Rev. B **47**, 14 988 (1993).

[5]E. Bucher, W. E. Brinkman, J. P. Maita, and H. J. Williams, Phys. Rev. Lett. **18**, 1125 (1968).

[6]A. Narath and A. T. Weaver, Phys. Rev. B **3**, 616 (1971).

[7]W. C. Muellner and J. S. Kouvel, Phys. Rev. B **11**, 4552 (1975).

[8]H. E. Mahnke, Hyperfine Interact. **49**, 77 (1989).

[9]V. V. Krishnamurthy, S. N. Mishra, Ravi Kumar, S. H. Devare, and H. G. Devare, Hyperfine Interact. (to be published).

[10]W. B. Pearson, *A Hand-Book of Lattice Spacings and Structures of Metals and Alloys* (Pergamon, Oxford, 1967), Vol. 2, p. 1134.

[11]H. Frauenfelder and R. M. Steffen, in *Alpha-, Beta- and Gamma-ray Spectroscopy,* edited by K. Sieghbahn (North-Holland, Amsterdam, 1965), Vol. 2, p. 997.

[12]H. Cottet, P. Donze, J. Ortelli, E. Walker, and M. Peter, Helv. Phys. Acta **41**, 755 (1968).

[13]V. L. Moruzzi, J. F. Janak, and A. R. Williams, *Calculated Electronic Properties of Metals* (Pergamon, New York, 1978).

[14]R. E. Watson and A. J. Freeman, in *Hyperfine Interactions,* edited by A. J. Freeman and R. B. Frankel (Academic, New York, 1967), p. 53.

[15]See the review by J. Callaway and N. H. March, in *Solid State Physics,* edited by H. Ehrenreich and D. Turnbull (Academic, New York, 1984), Vol. 38.

[16]D. E. Ellis and G. S. Painter, Phys. Rev. B **2**, 2887 (1970); E. J. Baerends, D. E. Ellis, and P. Ros, Chem. Phys. **2**, 41 (1973).

[17]J. van der Rest, F. Gautier, F. Brouers, J. Phys. F **5**, 995 (1975); Shigeru Hirooka and Masao Shimizu, J. Phys. Soc. Jpn. **43**, 477 (1977).

[18]D. Guenzburger and D. E. Ellis, Phys. Rev. Lett. **67**, 3832 (1991); D. Guenzburger and D. E. Ellis, Phys. Rev. B **45**, 285 (1992).

[19]R. Zeller, J. Phys. F **17**, 2123 (1987).

[20]S. Blügel, H. Akai, R. Zeller, and P. H. Dederichs, Phys. Rev. B **35**, 3271 (1987).

[21]P. L. Paulose, V. Nagarajan, R. Nagarajan, and R. Vijayaraghavan, Phys. Rev. B **42**, 1070 (1990).